

# Electrical Properties Analysis of Dielectric Thin Films $0.2\text{BaTiO}_3 - 0.8\text{BaZr}_{0.5}\text{Ti}_{0.5}\text{O}_3$ on Fluorine Doped Tin Oxide Substrate

Rahmi Dewi<sup>a\*</sup> , Nursyafni<sup>a</sup>, Siti Rahma Daulay<sup>a</sup>, Teguh P. Hadilala<sup>a</sup>, Sri Ningsih Sitorus<sup>a</sup>,  
Zulfa Nasir<sup>a</sup>, Ari Sulisty Rini<sup>a</sup>, Yanuar Hamzah<sup>a</sup>, Zuhdi<sup>b</sup>

<sup>a</sup>Universitas Riau, Faculty of Mathematics and Natural Sciences, Department of Physics, Pekanbaru, Indonesia.

<sup>b</sup>Universitas Riau, Faculty of Teacher Training and Education, Pekanbaru, Indonesia.

Received: August 05, 2023; Revised: November 13, 2023; Accepted: November 25, 2023

Ferroelectric thin films of  $0.2\text{BaTiO}_3 - 0.8\text{BaZr}_{0.5}\text{Ti}_{0.5}\text{O}_3$  (BT-BZT) are dielectric materials applied in various sensors, particularly in capacitor manufacturing, due to their excellent electrical properties. This ferroelectric material also has a high dielectric constant value, such that it is suitable for use in Ferroelectric Random Access Memory (FeRAM) and microwaves. Therefore, this study aimed to synthesize thin BT-BZT films with annealing temperature variations of 700 °C, 750 °C, and 800 °C. To achieve this, the sol-gel method was applied to Fluorine Doped Tin Oxide (FTO) substrate, a selected technique for its simplicity and cost-effectiveness. The electrochemical properties were characterized using electrochemical impedance spectroscopy (EIS). The research results show that at a frequency of 100 Hz, the highest dielectric constant obtained was 58975.43 at a temperature of 800 °C. This temperature has the highest resistance compared to other samples. The highest capacitance value is 2.9  $\mu\text{F}$  at a temperature of 700 °C. Therefore, it was concluded that the annealing temperature influenced the dielectric constant and the capacitance values of the capacitor.

**Keywords:** *Thin film, sol-gel method, dielectric constant, capacitance.*

## 1. Introduction

Thin films have been a subject of study for a century, and over time, they have proven valuable in the fields of science and technology<sup>1</sup>. The demand for nanoscale electronic components has been driven by technological advancements, particularly in the development of semiconductor devices such as diodes, capacitors, and transistors<sup>2</sup>. One notable application of thin films is in electrochemical sensors, where they serve as gas sensors capable of generating electrical signals in response to changes in the chemical environment<sup>3</sup>. The versatility extends across various scientific fields. In electronics, thin films are used to create capacitors, semiconductors, and sensors<sup>4</sup>, and are applied to enhance the corrosion resistance of metallic material in the field of construction<sup>5</sup>. These films are employed for decorative purposes, enhancing the aesthetics of homes, jewelry, and other accessories, thereby adding to their appealing nature.

Thin films were generally characterized by their electrical and optical properties, which often differed from the state of the constituent material<sup>6</sup>. One of the notable features was the relatively low electrical resistance, making them good electrical conductors<sup>7</sup>. Additionally, the optical properties commonly studied were transmission and absorbance<sup>8</sup>. In addition to the good electrical properties, thin films also possessed a conductive layer with high capability for transmitting visible and infrared light. These favorable electrical and optical properties led to their wide application across various fields<sup>9</sup>.

$\text{BaTiO}_3$  (BT), a ferroelectric material, has been extensively studied due to its unique properties, including the ability to store electric charge in a specific state and to preserve the charge even after the electric field is on or off. Additionally, BT has garnered attention as a lead (Pb)-free alternative due to the negative environmental impact of lead in electronic applications. Zirconium (Zr)-doped BT exhibits superior ferroelectric properties compared to pure BT. The properties are attributed to the  $\text{Zr}^{4+}$  ions replacing  $\text{Ti}^{4+}$  ions in the BT crystal structure, altering the material's polarization and enhancing its ferroelectric properties. Zr-doped BT possesses unique ferroelectric properties, making it suitable for various applications, such as memory, capacitors, and sensors<sup>10</sup>. Studies have demonstrated that the introduction of Zr atoms to replace Ti atoms in BT enhances the electrical, optical, and other properties of BT<sup>11</sup>. Since the ionic radius of Zr is larger than that of Ti, this leads to a more stable crystal structure. When Zr atoms replace Ti atoms in the BT crystal structure, changes occur in the crystal lattice parameters, leading to a more stable crystal structure. Additionally, Zr atoms can influence the ferroelectric properties of BT. In this study, the combination of dielectric material BT-BZT provides a high dielectric constant. The temperature and dielectric constant influence the compatibility of the dielectric material<sup>12</sup>. Various techniques to synthesize nanostructured BT-BZT have been developed, such as solid-state reactions, traditional mixed oxide methods, ball milling, and sol-gel methods<sup>11</sup>. Because of its easy application and cost-effectiveness, the sol-gel method was preferred compared to the other methods.

\*e-mail: [drahmi2002@yahoo.com](mailto:drahmi2002@yahoo.com)

Furthermore, the effect of annealing temperature on the electrochemical properties of BT-BZT was characterized using electrochemical impedance spectroscopy (EIS). EIS is a potent analytical technique employed in studying the behavior of electrochemical systems<sup>13-15</sup>. It involved applying a low-amplitude *alternating current* (AC) signal to the system and analyzing the resulting voltage response. By controlling the AC signal frequency within a certain range, this technique enables impedance measurements as a function of frequency. EIS provides information about the electrical properties of the system, including resistance, capacitance, and inductance, as well as other electrochemical properties, such as charge transfer resistance, double-layer capacitance, and diffusion coefficients<sup>16,17</sup>. This technique can also be used to study the kinetics and mechanisms of electrochemical reactions, species adsorption on electrode surfaces, and the behavior of complex electrochemical systems<sup>18</sup>. EIS is a valuable tool for characterizing and understanding electrochemical systems due to its non-invasive and non-destructive nature, providing information about their electrical and electrochemical properties<sup>19,20</sup>.

This research uses a mixture of BT and BZT materials with a composition of  $0.2\text{BaTiO}_3 - 0.8\text{BaZr}_{0.5}\text{Ti}_{0.5}\text{O}_3$ . The resulting solution was deposited on a *Fluorine Doped Tin Oxide* (FTO) substrate and subjected to a spin coating and annealing process at temperatures of 700 °C, 750 °C, and 800 °C to improve the electrical properties. Results from the X-ray diffraction (XRD) and field emission scanning electron microscope (FESEM) characterization showed that the crystal structure is cubic and the grain size increases with increasing annealing temperature<sup>11</sup>. Furthermore, the samples were characterized using impedance spectroscopy to determine the dielectric constant and capacitance values of the BT-BZT material.

## 2. Methods

BT-BZT was synthesized through the sol-gel method, and the materials used were Merck Barium Carbonate ( $\text{BaCO}_3$ ) powder, Titanium Dioxide ( $\text{TiO}_2$ ), and Zirconium Carbonate ( $\text{ZrCO}_2$ ) with 99%, 99%, and 98% purity, respectively. The materials were weighed and mixed with their respective solvents. These included 3 ml of acetic acid and 2 ml of deionized water, as well as ethylene glycol and alcohol, for  $\text{ZrCO}_2$  and  $\text{TiO}_2$  powder, respectively.  $\text{BaCO}_3$  was mixed with the Zr and Ti solutions, before adding 3 drops of acetylacetone. The mixture was stirred using a magnetic stirrer on a hot plate at 250 rpm and 31.6 °C for 2 hours until achieving clarity, resulting in the formation of the BZT solvent. Subsequently, BT-BZT material was dissolved in a mixture of 20:80 deionized water and acetic acid. Both components were stirred, and acetylacetone was added as a stabilizing agent. The stirring continued until a clear yellowish color was obtained. To remove water and inorganic impurities, the sample was heated for 15 minutes at 150 °C and 350 °C after spin coating at 3500 rpm for 30 seconds on an FTO substrate<sup>11</sup>. Finally, annealing was conducted at 700 °C, 750 °C, and 800 °C, while the electrochemical properties were characterized using EIS.

## 3. Results and Discussion

EIS characterization was the most effective method for studying the chemical properties and physical processes occurring at the electrode interface. Through this testing approach, values of capacitance, impedance, charge transfer rate, and resistance were obtained<sup>21</sup>.

To investigate the charge transfer kinetics, EIS testing was conducted, and a Nyquist plot was obtained. The Nyquist plot indicated the variation between real  $Z'$  and imaginary impedance  $Z''$  over a frequency range from 50 Hz to 1 MHz for all samples, as shown in Figure 1.

Figure 1 shows the insert representation of the corresponding circuit used to adjust data at annealing temperatures of 700 °C, 750 °C, and 800 °C. The Zsimpwin software is used to fit various optimal models to experimental data. Table 1 lists resistance and capacitance values at different temperatures are provided in the Nyquist plot typically has several half-circle arcs, where the first circle observed at higher frequencies represents the grain effect. The presence of intermediate frequencies indicated the influence of grain boundaries, represented by the second circle. The third circle at lower frequency regions represented the electrode effect<sup>20</sup>. According to Figure 1, all BT-BZT samples exhibited half-circle patterns indicating charge transfer resistance<sup>22</sup>. BT-BZT800 sample had a larger half-circle than the others, indicating higher charge transfer resistance.

BT-BZT700 displays a smaller semicircle, indicating the lowest charge transfer resistance and implying faster charge transfer kinetics<sup>23,24</sup>. High annealing temperature affects the resistance because of the formation or migration of certain defects perturbing electrical charge movement<sup>25</sup>. Complex impedance  $|z|$  was utilized to determine the resistive or capacitive contribution to the material conductivity when subjected to an alternating current electric field.

Figure 2 shows the results of complex impedance measurements of BT-BZT in the frequency range from 50 Hz to 1 MHz. In Figure 2a, all  $Z'$  values remained stable at lower frequencies and decreased as the frequency increases. The decrease in their values indicated an increase in BT-BZT conductivity<sup>24</sup>. The graph of the imaginary impedance component ( $Z''$ ) against frequency is presented in Figure 2b. Additionally, the single peak present in this plot indicated the occurrence of a single dielectric relaxation process in the BT-BZT sample. This process arises due to the interface effect<sup>26</sup>.

The Bode phase plot showed the phase shift with frequency for each sample variation, as indicated in Figure 3.

Furthermore, as the frequency log value increased, the  $|z|$  value decreased for the three sample variations, as shown in Figure 4.

Figure 5a showed a consistent pattern for all compositions, with a higher dielectric constant in the low-frequency region (100 Hz). However, as the frequency increased up to 1 MHz, the dielectric constant rapidly decreased to a constant level. Different polarization mechanisms, such as ionic, dipolar, electronic, and space charges, significantly impacted the dielectric constant. At low frequencies, electric dipoles within the compound aligned with the applied electric field, resulting in total sample polarization.

In this region, almost all polarizations became prominent<sup>27</sup>, but as the frequency increased to 1 MHz, their contribution gradually decreased except for electronic polarization, leading to a low dielectric constant. The rapid changes in the electric

field at high frequencies make it difficult for electrons to follow, causing alterations in their movement and reducing the accumulation of charges at the grain boundaries of the dielectric material. As a result, the dielectric constant value decreased<sup>26</sup>.

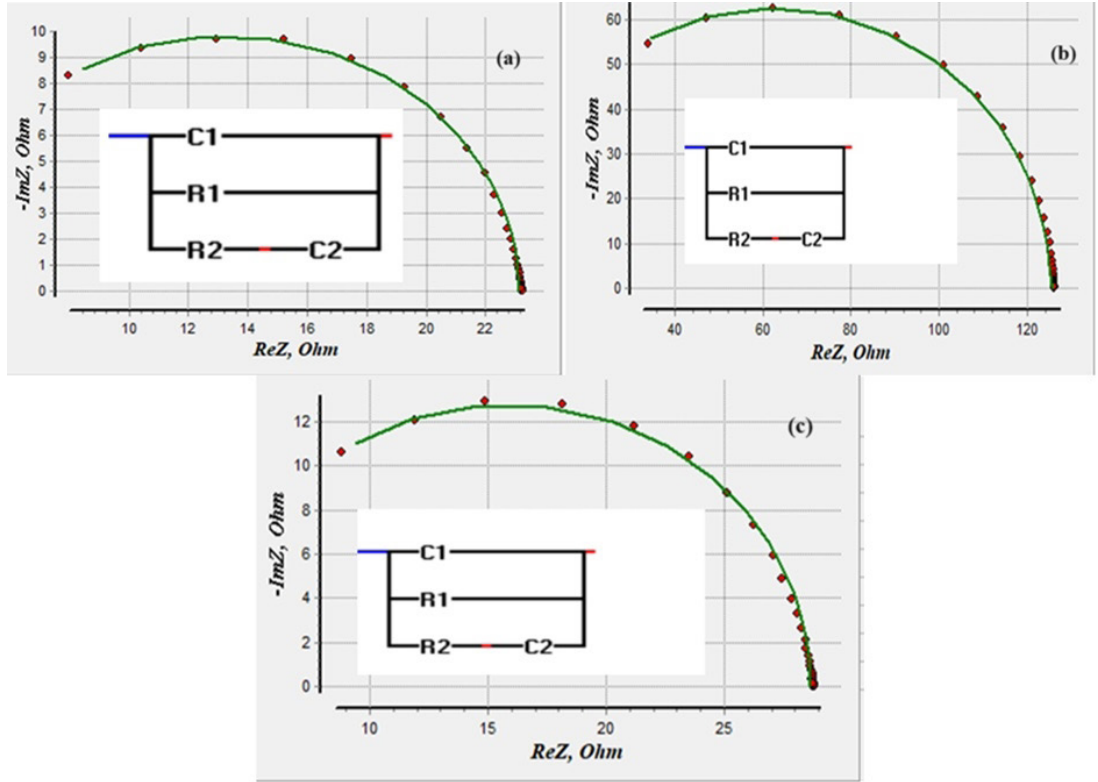


**Figure 1.** Nyquist plot and equivalent circuit model for BZ-BZT sample at annealing temperatures of (a) 700 °C, (b) 750 °C, and (c) 800 °C.

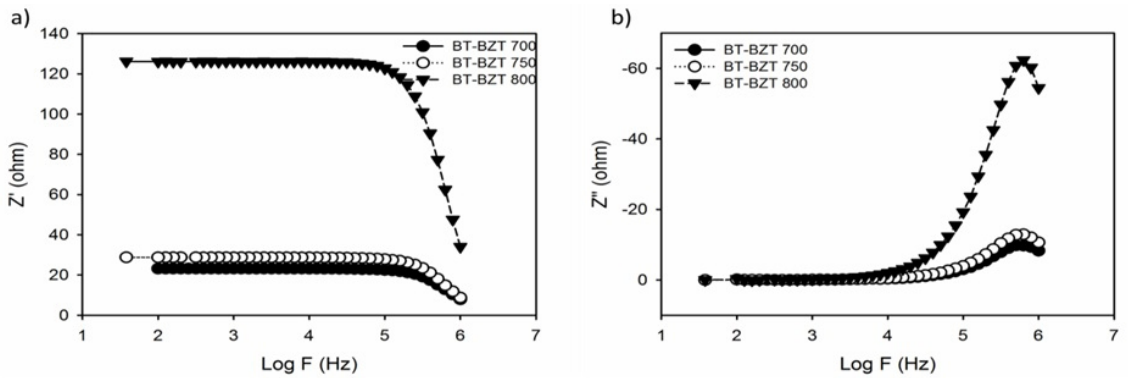


**Figure 2.** The relationship between (a) real  $Z'$  and (b) imaginary  $Z''$  impedance with respect to frequency with variations in annealing temperature.

**Table 1.** The value of the electrical circuit elements  $R_1$ ,  $R_2$ ,  $C_1$  and  $C_2$  to the impedance of each sample.

Sample	$R_1$ ( $\Omega$ )	$R_2$ ( $\Omega$ )	$C_1$ (nF)	$C_2$ ( $\mu\text{F}$ )
BT-BZT700	10000	10000	2000	2000
BT-BZT750	29.76	7.45	2.5	5.8
BT-BZT800	58.78	29.73	2.5	1.6

These values are calculated using equations described in the study conducted by Saadi et al.<sup>28</sup>. The higher the annealing temperature, the larger the dielectric constant. Samples annealed at temperatures of 700 °C, 750 °C, and 800 °C obtained dielectric constant values at 100 Hz, namely 22550.17, 29926.6, and 58975.43, respectively. The high dielectric constant is because, at higher temperatures, molecules in the dielectric material can experience greater polarization. The polarization can enhance the dielectric constant due to the emersion of high dipole moments<sup>29-31</sup>. The dielectric constant value of BT-BZT is much increased compared to research conducted by Dewi et al.<sup>32</sup>, which only used BZT material.

Figure 5b shows the dielectric loss of all BT-BZT samples in the range of frequencies of 100 Hz to 1 MHz.

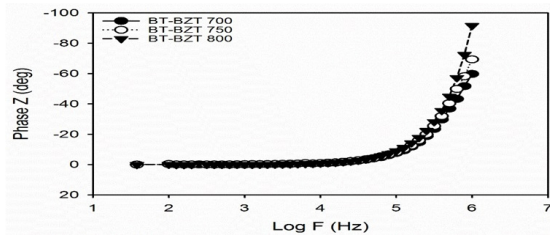


**Figure 3.** Bode phase plot for BZ-BZT sample with variations in annealing temperature.

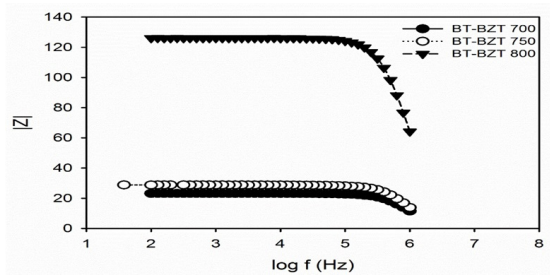


**Figure 4.** Graphic of the relationship between  $|Z|$  against  $\log f$  for BZ-BZT sample with variations in annealing temperature.

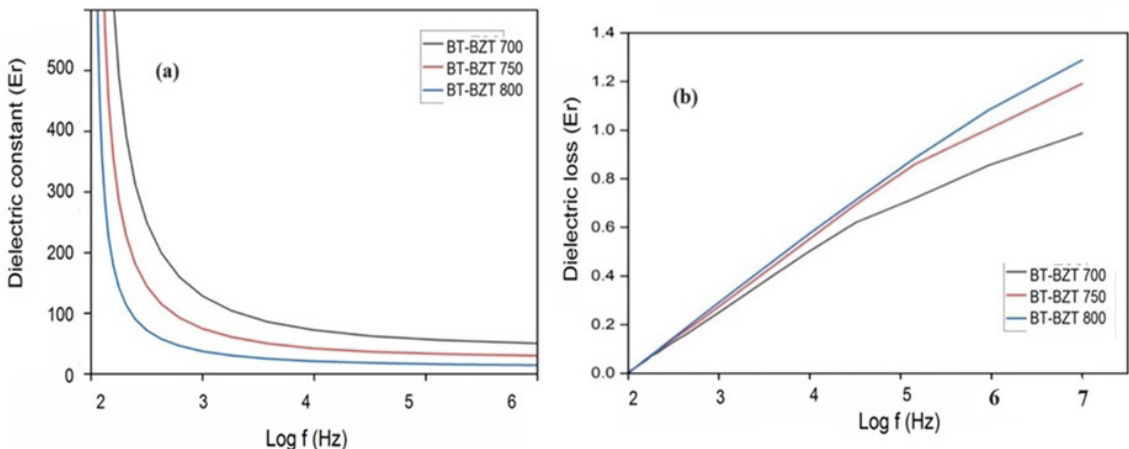


**Figure 5.** Graph of the relationship between (a) dielectric constant and  $\log f$  (b) dielectric loss and  $\log f$  at different annealing temperatures.

In addition, it is observed that when the annealing temperature increases up to BT-BZT800, the dielectric loss also increases with the increase in frequency. Several factors determine the increased dielectric loss due to the increased frequency. Firstly, the time available for molecules in the dielectric material to respond to changes in the electric field becomes shorter at higher frequencies. The short time causes increased frictional forces and heat generation, leading to high dielectric losses. Secondly, material defects due to imperfections or disturbances in the material structure, the replacement of original atoms with another type of atoms in the crystal structure<sup>30,33</sup>. The surface morphology of the material with increasing annealing temperature shows an increasing grain size. Surface morphology is in the form of irregularly shaped spheres. The grain sizes at annealing temperatures of 700 °C, 750 °C, and 800 °C are as follows:  $205.83 \pm 48.34$  nm,  $252.53 \pm 68.66$  nm, and  $292.43 \pm 50.69$  nm, respectively. Samples annealed at 800 °C have larger grain sizes than other samples. This result is by the XRD pattern peak with a cubic structure, where the material crystallinity increases with increasing annealing temperature. The Full width at half maximum (FWHM) was measured from the top (001) at 700 °C, 750 °C, and 800 °C at 2.203, 1.801, and 1.184, respectively<sup>11</sup>. Loss of dielectric increases with the increasing annealing temperature. The charge transfer kinetics increase with temperature and increase polarization, which results in high dielectric losses. Charge accumulation at grain boundaries caused high dielectric losses at higher temperatures<sup>29,30,32</sup>.

Figure 6 shows the capacitance of each sample based on the annealing temperature variation. Furthermore, it was observed that the capacitance showed an inverse relationship with both the annealing temperature and the frequency<sup>34</sup>. As discussed in the Nyquist plot, the BT-BZT800 sample shows a higher charge transfer resistance than the other samples, resulting in a smaller capacitance. Among the samples tested, the BT-BZT700 showed the lowest resistance with a capacitance value of  $2.9 \mu\text{F}$ , facilitating faster charge transfer. This BT-BZT capacitance value is higher than the BZT capacitance value in nano Farad units carried out by Dewi et al.<sup>32</sup>.

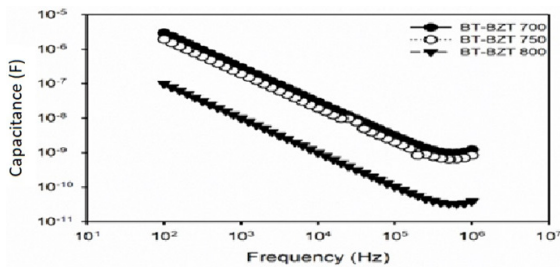


**Figure 6.** Graph of the relationship between capacitance and frequency with variations in annealing temperature.

## 4. Conclusion

In conclusion, BT-BZT dielectric material was successfully produced using various annealing temperatures of 700 °C, 750 °C, and 800 °C. Based on the EIS analysis, the sample annealed at 700 °C exhibited the highest capacitance and the lowest resistance. Furthermore, the study revealed a clear relationship between temperature variation and electrical properties. As the temperature increased, the capacitance decreased, and the resistance increased. The highest value recorded for the dielectric constant at an annealing temperature of 800 °C is 58975.43. The capacitance value at an annealing temperature of 700 °C is 2.9  $\mu\text{F}$ . Based on the results obtained, the annealing temperature has a significant effect on the dielectric constant value and capacitance value of the capacitor.

## 5. Acknowledgments

Rahmi Dewi acknowledges the financial support from the collaboration between the National Research Agency (BRIN) and the Education Fund Management Institute (LPDP) with the Institute for Research and Community Service, Riau University (LPPM-UNRI) funding number 82/II.7/HK/2022.

## 6. References

- Bala N, Khan B, Singh K, Singh P, Singh AP, Thakur A. Recent advances in doped  $\text{Ge}_2\text{Sb}_2\text{Te}_5$  thin film based phase change memories. *Mater. Adv.* 2023;4(3):747-68. <http://dx.doi.org/10.1039/D2MA01047J>.
- Malik S, Muhammad K, Waheed Y. Nanotechnology: a revolution in modern industry. *Molecules.* 2023;28(2):661. <http://dx.doi.org/10.3390/molecules28020661>.
- Zhang T, Yao G, Pan T, Lu Q, Lin Y. Flexible inorganic oxide thin-film electronics enabled by advanced strategies. *J Semicond.* 2020;41(4):041602. <http://dx.doi.org/10.1088/1674-4926/41/4/041602>.
- Catania F, Oliveira HS, Lugoda P, Cantarella G, Münzenrieder N. Thin-film electronics on active substrates: review of materials, technologies and applications. *J Phys D Appl Phys.* 2022;55(32):323002. <http://dx.doi.org/10.1088/1361-6463/ac6af4>.
- Shao G, Hanaor DAH, Shen X, Gurlu A. Freeze casting: from low-dimensional building blocks to aligned porous structures: a review of novel materials, methods, and applications. *Adv Mater.* 2020;32(17):1907176. <http://dx.doi.org/10.1002/adma.201907176>.
- Nguyen PTM, Nguyen T, Nguyen MD, Vu TH. Impact of electrode materials on microstructure, leakage current and dielectric tunable properties of lead-free BSZT thin films. *Ceram Int.* 2021;47(16):23214-21. <http://dx.doi.org/10.1016/j.ceramint.2021.05.033>.
- Triana-Camacho DA, Quintero-Orozco JH, Mejía-Ospino E, Castillo-López G, García-Macías E. Piezoelectric composite cements: towards the development of self-powered and self-diagnostic materials. *Cement Concr Compos.* 2023;139:105063. <http://dx.doi.org/10.1016/j.cemconcomp.2023.105063>.
- Sandi DK, Iriani Y, Fasquelle D. Microstructure and optical properties of Zirconium Co-Doped Barium Titanate thin films on quartz substrates. *Key Eng Mater.* 2022;907:44-9. <http://dx.doi.org/10.4028/www.scientific.net/KEM.907.44>.
- Song JH, Min SH, Kim SG, Cho Y, Ahn H. Multi-functionalization strategies using nanomaterials: a review and case study in sensing applications. *Int J Precis Eng Manuf Green Technol.* 2022;9(1):323-47. <http://dx.doi.org/10.1007/s40684-021-00356-1>.
- Thanachayanont C, Yordsri V, Kijamnajsuk S, Binhayeeniyi N, Muensit N. Microstructural investigation of sol-gel BZT powders. *Mater Lett.* 2012;82:205-7. <http://dx.doi.org/10.1016/j.matlet.2012.05.075>.
- Dewi R, Luqman TS, Sitorus SN, Vitayaya O, Rini AS, Zuhdi. The effect of annealing temperature on microstructure and energy band gap of  $0.2\text{BaTiO}_3 - 0.8\text{BaZr}_{0.5}\text{Ti}_{0.5}\text{O}_3$  nano material. *Mater Today Proc.* 2023;87:159-63. <http://dx.doi.org/10.1016/j.matpr.2023.02.391>.
- Gatea HA. Effect of substrate-induced strains on ferroelectric and dielectric properties of lead zirconate titanate films prepared by the sol-gel technique. *Nanosci Nanotechnol Asia.* 2020;11(3):322-9. <http://dx.doi.org/10.2174/221068121099200715105250>.
- Lazanas AC, Prodromidis MI. Electrochemical impedance spectroscopy: a tutorial. *ACS Meas. Sci. Au.* 2023;3(3):162-93. <http://dx.doi.org/10.1021/acsmesuresciau.2c00070>.
- Vadhva P, Hu J, Johnson MJ, Stocker R, Braglia M, Brett DJL, et al. Electrochemical impedance spectroscopy for all-solid-state batteries: theory, methods and future outlook. *ChemElectroChem.* 2021;8(11):1930-47. <http://dx.doi.org/10.1002/celec.202100108>.
- Middlemiss LA, Rennie AJR, Sayers R, West AR. Characterisation of batteries by electrochemical impedance spectroscopy. *Energy Rep.* 2020;6:232-41. <http://dx.doi.org/10.1016/j.egyr.2020.03.029>.
- Ma Z, Dacayan WL, Chatzichristodoulou C, Mølhavé KS, Chiabrera FM, Zhang W, et al. Electrochemical Impedance spectroscopy integrated with environmental transmission electron microscopy. *Small Methods.* 2023;7(7):e2201713. <http://dx.doi.org/10.1002/smt.202201713>.
- Deyab MA, El-Shamy OAA, Thabet HK, Ashmawy AM. Electrochemical and theoretical investigations of favipiravir drug performance as ecologically benign corrosion inhibitor for aluminum alloy in acid solution. *Sci Rep.* 2023;13(1):8680. <http://dx.doi.org/10.1038/s41598-023-35226-0>.
- Da Silva LM, De Sousa LG, Vicentini R, Aguiar JP, Doubek G, Zanin H. Proposal of a novel methodology for the electrochemical characterization of well-behaved redox-active materials used in supercapacitors. *Electrochim Acta.* 2023;457:142458. <http://dx.doi.org/10.1016/j.electacta.2023.142458>.
- Savva A, Saez J, Withers A, Barberio C, Stoeger V, Elias-Kirma S, et al. 3D organic bioelectronics for electrical monitoring of human adult stem cells†. *Mater Horiz.* 2023;10(9):3589-600. <http://dx.doi.org/10.1039/D3MH00785E>.
- Brito-Garcia SJ, Mirza-Rosca JC, Jimenez-Marcos C, Voiculescu I. EIS study of doped high-entropy alloy. *Metals.* 2023;13(5):883. <http://dx.doi.org/10.3390/met13050883>.
- Ramohlola KE, Iwuoha EI, Hato MJ, Modibane KD. Instrumental techniques for characterization of molybdenum disulphide nanostructures. *J Anal Methods Chem.* 2020;2020:8896698. <http://dx.doi.org/10.1155/2020/8896698>.
- Khan H, Pawar RC, Charles H, Changula PJ, Lee CS. One-pot synthesis of octahedral  $\text{NiSe}_2$  as a co-catalyst for enhanced  $\text{CO}_2$  photoreduction performance. *Appl Surf Sci.* 2023;629:157362. <http://dx.doi.org/10.1016/j.apsusc.2023.157362>.

23. Chen J, Gu Y, Xu S, Zhang Y, Zhang Z, Shi L, et al. Band gap engineering in quadruple-layered Sillén-Aurivillius perovskite oxychlorides  $\text{Bi}_7\text{Fe}_2\text{Ti}_2\text{O}_{17}\text{X}$  ( $\text{X} = \text{Cl}, \text{Br}, \text{I}$ ) for enhanced photocatalytic performance. *Catalysts*. 2023;13(4):751. <http://dx.doi.org/10.3390/catal13040751>.
24. Urgesa MH, Wolde GS, Kuo D-H. One-step hydrothermal synthesis of novel flower-like  $\text{Bi}_2\text{Mn}_4\text{O}_{10}$  anchored on  $\text{BiOI}_{1-x}\text{Br}_x$  nanosheets for efficient photocatalytic nitrogen fixation. *J Alloys Compd*. 2023;947:169589. <http://dx.doi.org/10.1016/j.jallcom.2023.169589>.
25. Park K, Zhang Q, Garcia BB, Cao G. Effect of annealing temperature on  $\text{TiO}_2$ -ZnO core-shell aggregate photoelectrodes of dye-sensitized solar cells. *J Phys Chem C*. 2011;115(11):4927-34. <http://dx.doi.org/10.1021/jp110872k>.
26. Mohamed Saadon NAF, Taib NI, Loy CW, Mohamed Z. Role of  $\text{Ca}^{2+}$  doping on the enhancement of dielectric properties of  $\text{Sr}_{2-x}\text{Ca}_x\text{NiWO}_6$  for energy storage device application. *Sci Rep*. 2023;13(1):1246. <http://dx.doi.org/10.1038/s41598-023-28296-7>.
27. Venkatesh N, Kumar DR, Goud S, Ahmad SI, Veerasomaiah P, Ravinder D. Structural, photocatalytic, electromagnetic properties of rare-earth metal Gd-doped Mg nanoferrites synthesized by citrate gel auto-combustion method. *Chem Zvesti*. 2023;77(5):2749-67. <http://dx.doi.org/10.1007/s11696-023-02664-z>.
28. Saadi H, Benzarti Z, Sanguino P, Hadouch Y, Mezzane D, Khirouni K, et al. Improving the optical, electrical and dielectric characteristics of ZnO nanoparticles through (Fe + Al) addition for optoelectronic applications. *Appl Phys, A Mater Sci Process*. 2022;128(8):691. <http://dx.doi.org/10.1007/s00339-022-05847-9>.
29. Koab J, Bouguila N, Abassi H, Moutia N, Kraini M, Timoumi A, et al. Dielectric and electrical properties of annealed ZnS thin films: the appearance of the OLPT conduction mechanism in chalcogenides. *RSC Advances*. 2020;10(16):9549-62. <http://dx.doi.org/10.1039/C9RA10284A>.
30. Sahoo S, Hajra S, De M, Mohanta K, Choudhary RNP. Processing, dielectric and impedance spectroscopy of lead free  $\text{BaTiO}_3$ - $\text{BiFeO}_3$ - $\text{CaSnO}_3$ . *J Alloys Compd*. 2018;766:25-32. <http://dx.doi.org/10.1016/j.jallcom.2018.06.284>.
31. Hajra S, Tripathy A, Panigrahi BK, Choudhary RNP. Development and excitation performance of lead free electronic material: Eu and Fe doped  $\text{Bi}_{0.5}\text{Na}_{0.5}\text{TiO}_3$  for filter application. *Mater Res Express*. 2019;6(7):076304. <http://dx.doi.org/10.1088/2053-1591/ab149b>.
32. Dewi R, Luqman TS, Hamzah Y, Krisman, Rini AS. The effect of heating rate on  $\text{BaZr}_x\text{Ti}_{1-x}\text{O}_3$  thin film for  $x=0.4$  and  $x=0.6$  as capacitors. *J Mater Res Technol*. 2022;18:3826-33. <http://dx.doi.org/10.1016/j.jmrt.2022.04.044>.
33. Šuljagić M, Petronijević I, Mirković MM, Kremenović A, Džunuzović A, Pavlović VB, et al.  $\text{BaTiO}_3/\text{Ni}_x\text{Zn}_{1-x}\text{Fe}_2\text{O}_4$  ( $x = 0, 0.5, 1$ ) composites synthesized by thermal decomposition: magnetic, dielectric and ferroelectric properties. *Inorganics*. 2023;11(2):51. <http://dx.doi.org/10.3390/inorganics11020051>.
34. Verma N, Jagota V, Alguno AC, Alimuddin, Rakhra M, Kumar P, et al. Characterization of fabricated gold-doped ZnO nanospheres and their use as a photocatalyst in the degradation of DR-31 dye. *J Nanomater*. 2022;2022:7532332. <http://dx.doi.org/10.1155/2022/7532332>.